We are IntechOpen, the world's leading publisher of Open Access books Built by scientists, for scientists

4,800
Open access books available

122,000
International authors and editors

135M
Downloads

Our authors are among the

154
Countries delivered to

TOP 1%
most cited scientists

12.2%
Contributors from top 500 universities

CLARIVATE ANALYTICS BOOK CITATION INDEX INDEXED

WEB OF SCIENCE™

Selection of our books indexed in the Book Citation Index in Web of Science™ Core Collection (BKCI)

Interested in publishing with us?
Contact book.department@intechopen.com

Numbers displayed above are based on latest data collected.
For more information visit www.intechopen.com

9

A Concept of Discretization Error Indicator for Simulating Thermal Radiation by Finite Volume Method Based on an Entropy Generation Approach

H. C. Zhang, Y. Y. Guo, H. P. Tan and Y. Li
Harbin Institute of Technology
P. R. China

1. Introduction

Heat transfer is frequently dominated by Thermal Radiation (TR) in many scientific and engineering applications, especially at high temperature (Howell et al., 2010). Usually, three main fundamental approaches are supplemented to investigate TR problem, including analytical, experimental and numerical methods (Modest, 2003), however, among those TR problems, only quite a few of them can be analytically or experimentally solved. Recently, because of a rapid growth of computer and information techniques, numerical approximation has been eventually become the major simulating tool towards TR problems. The general equation to describe TR transport is the Radiative Transfer Equation (RTE), and several computational algorithms were proposed for solution of the RTE, which have achieved great advancement (Howell et al., 2010; Modest, 2003; Shih et al., 2010).

The Finite Volume Method (FVM) has validated to be an efficient algorithm with satisfactory precision (Raithby & Chui, 1990), which has been applied to various problems. Besides, much innovation to improve its performance is also proposed. FTn method is used to predict TR characteristics for a 3D complex industrial boiler with non-gray media (Borjini et al., 2007). FVM is applied with Lattice Boltzmann method in a transient 2D coupled conduction-radiation problem by an inverse analysis (Das et al., 2008). Combined mixed convection-radiation heat transfer is dealt with by a FVM (Farzad & Shahini, 2009). Transient radiative heating characteristics of slabs in a walking beam type reheating furnace is predicted by FVM (Han et al., 2009). A complex axisymmetric enclosure with participating medium is investigated by using FVM with an implementation of the unstructured polygonal meshes (Kim et al., 2010). A particular procedure as a first-order skew, positive coefficient, upwind scheme was presented (Daniel & Fatmir, 2011), which is incorporated in FVM.

Essentially, FVM can be categorized as a numerical method applied to investigate radiative heat transfer problems. Because algebraic equations for the FVM are determined through discretization of the RTE over user-selected control volumes and specific control solid angles, it will inevitably encounter various errors, which is an important and integral part in connection with the solution procedures. The most common discretization errors occurring in the FVM are called the ray effect and the false scattering, which were initially identified

by Chai et al. (Chai et al., 1993). Only the error caused by spatial discretization is discussed in this paper, and it is also referred to as numerical scattering or numerical smearing (Zhang & Tan, 2009), which is analogous to false diffusion in the context of computational fluid dynamics caused by discretization of spatial coordinates (Patankar, 1980). It has been shown that many factors can cause false scattering (Tan et al., 2004) influencing solution accuracy, including grid quality (Kallinderis & Kontzialis, 2009), spatial discretization schemes (Coelho, 2008), radiative properties and volumetric heat sources (Kamel et al., 2006). However, there are few effective routines for evaluating the spatial discretization error, and it is necessary to formulate an innovative framework to explore parameters or define indicator to analyze its uncertainty and accuracy.

The concept and theory of entropy, based on the second law of thermodynamics, has been an innovative and effective approach to study computational errors within the fields of fluid flow and heat transfer (Naterer & Camberos, 2003). The entropy production is used to predict numerical errors for viscous compressible flow (Camberos, 2000). The concept of information entropy (Cover & Thomas, 2003) has been shown to be an appropriate method and has been widely applied to error analysis for Euler's equations and the stability of numerical solution (Camberos, 2007). Although some work has been done based on radiation entropy generation (Caldas & Semiao, 2005; Liu & Chu, 2007), much work has been focused on error analysis in computational fluid dynamics, heat conduction and heat convection, instead of error analysis for TR. In the previous work, an entropy formula based on information theory is proposed to investigate uncertainty in FVM towards artificial benchmarks (Zhang et al. 2011), which show its adaptability in field of TR.

In this chapter, an artificial benchmark model of central laser incidence on a two-dimensional (2D) rectangle containing a semi-transparent medium is used as a framework to investigate the numerical scattering, using reference data from the Monte Carlo method (MCM), which has been proven to generate no false scattering (Tan et al., 2004). Based on the local entropy generation approach (Herwig & Kock, 2004) derived from the second law of thermodynamics, which is considered a very effective method to analyze the process of energy transfer, a discretization error indicator is defined. Within the framework of the current model, grid independence is first validated. The effects of the spatial differential scheme, the spatial grid number and the absorption coefficient deviation of the medium on numerical scattering in the FVM are presented.

2. Mathematical model and artificial benchmark

In an emitting, absorption and scattering medium, the RTE can be written as:

$$\frac{\mathrm{d}I_\lambda\left(\vec{s},\vec{\Omega}\right)}{\mathrm{d}s}=-\kappa_{\alpha\lambda}I_\lambda\left(\vec{s},\vec{\Omega}\right)-\kappa_{s\lambda}I_\lambda\left(\vec{s},\vec{\Omega}\right)+\kappa_{\alpha\lambda}I_{b\lambda}\left(\vec{s}\right)+\frac{\kappa_{s\lambda}}{4\pi}\int_{4\pi}I_\lambda\left(\vec{s},\vec{\Omega}'\right)\Phi_\lambda\left(\vec{\Omega}',\vec{\Omega}\right)\mathrm{d}\Omega' \quad (1)$$

For an opaque, diffuse emitting and reflective boundary wall, the corresponding boundary condition can be written as:

$$I_\lambda\left(\vec{\Omega}\right)=\varepsilon_\lambda I_{b\lambda}+\frac{1-\varepsilon_\lambda}{\pi}\int_{\vec{n}_b\cdot\vec{\Omega}'<0}I_\lambda\left(\vec{\Omega}'\right)|\,\vec{n}_b\bullet\vec{\Omega}'\,|\,d\vec{\Omega}' \quad (2)$$

When FVM is used to solve the RTE, hemispherical space of 4π steradians is divided to a solid angular grid, i.e., a limited number of directions. Along a specific angular direction Ω^l, a relationship is necessary to correlate the radiative intensities at the face of the control volume to the intensity at the centre of control volume. This yields a spatial differential scheme, which in general can be represented as:

$$I_p^{\Omega^l} = \sum f_\alpha I_\beta^{\Omega^l} \tag{3}$$

where f_α denotes different values for f_x, f_y and f_z corresponding different types of differential schemes, and I_β means radiative intensities at different interfaces of a control volume, including I_e, I_w, I_n, I_s, I_t and I_b.

Frequently, the following three kinds of differencing schemes are selected, namely, the step scheme with $f_\alpha = 1.0$, the diamond scheme with $f_\alpha = 0.5$ and the exponential scheme with:

$$f_\alpha = \left[1 - \exp\left(-\tau_\alpha^{\Omega^l}\right)\right]^{-1} - \left(\tau_\alpha^{\Omega^l}\right)^{-1} \tag{4}$$

where τ is the optical thickness.

2.1 Numerical scattering

It is generally considered that numerical scattering is a multi-dimensional problem caused by spatial coordinates discretization. When the first term of the truncation error is the second-order space derivative, its error is dissipative. The derivative term of radiative intensity is used as the first-order difference scheme in the solution of RTE and truncation error is the second-order space derivative. As a result, numerical scattering is caused. Its premise is that: intensity at certain grids is related to other grids by space deferential schemes, and these grids are not in the transfer direction. In a multi-dimensional problem, if a derivative is substituted by first-order difference, if the profile of radiative intensity is assumed by spatial differencing schemes and if the direction of transfer is intersected with grid and non-negative intensity gratitude exists in the direction perpendicular with transportation direction, numerical scattering is still generated (Tan et al., 2004).

Because numerical scattering is a multi-dimensional problem, a 2D case is taken into account in the current study, without considering the scattering in the medium.

The accurate solution for the spectral radiative intensity in a specific angular direction Ω^l of the FVM is denoted by $I_{(\vec{s})}^{\Omega^l}$, and the symbol $L(I)_{\vec{s},\Omega^l}$ is defined as an operator for the differential process of $I_{(\vec{s})}^{\Omega^l}$ at a control volume of $\left(\vec{s},\Omega^l\right)$, where vector $\vec{s}$ denotes the spatial coordinates of the point, as shown in Eq. (5):

$$L(I)_{\vec{s},\Omega^l} = \left[\xi\frac{\partial I}{\partial x} + \eta\frac{\partial I}{\partial y} - \kappa_{\alpha\lambda} I - S\right]_{\vec{s},\Omega^l} \tag{5}$$

If the symbol $L_{\Delta\vec{s}}\left[I_{(\vec{s})}^{\Omega^l}\right]$ is used for the difference operator for $I_{(\vec{s})}^{\Omega^l}$, we then have:

$$L_{\Delta\vec{s}}\left[I_{(\vec{s})}^{\Omega^l}\right]=\xi\frac{I_{i+1}^{\Omega^l}-I_i^{\Omega^l}}{\Delta x}+\eta\frac{I_{j+1}^{\Omega^l}-I_j^{\Omega^l}}{\Delta y}-\kappa_{\alpha\lambda}I^{\Omega^l}-S_s^{\Omega^l} \tag{6}$$

In Eq. (6), $L_{\Delta\vec{s}}\left[I_{(\vec{s})}^{\Omega^l}\right]$ denotes the step scheme for a 2D differential equation. In this way, the cut-off for the discrete differential equations denotes the difference between the difference operators and the corresponding differential operators, which can be expressed using *TE*, i.e.

$$TE=L_{\Delta\vec{s}}\left[I_{(\vec{s})}^{\Omega^l}\right]-L(I)_{\vec{s},\,\Omega^l} \tag{7}$$

Eq. (7) can be deduced using the Taylor expansion of the difference equation. For the case above, the Taylor expansions of $I_{(\vec{s})}^{\Omega^l}$ and $I_{(\vec{s}+d\vec{s})}^{\Omega^l}$ in the space position $\vec{s}=\vec{s}(i,j)$ can be substituted into the difference equation and reorganized, and we then obtain the correlation function shown in Eq. (8):

$$TE=O\left(\Delta x^2,\Delta y^2\right)+\left(S_s^{\Omega^l}-S\Big|_{s,\,\Omega^l}\right) \tag{8}$$

For a 2D problem, if the derivative is substituted for a first-order difference, if the radiative intensity profile is assumed by the space differential schemes, and if the transfer direction intersects with the grid and a non-negative radiative intensity gradient exists in the direction perpendicular to the transportation direction, numerical scattering is still generated.

Generally, a relationship should be derived to correlate the radiative intensities in the face of the control volume and the intensities at the centre of the control volume, which constitute a kind of spatial differential scheme. In view of this, the numerical scattering is also related to the spatial differential factor, which is shown in Eq. (9):

$$TE=\left|\frac{\partial I^{\Omega^l}}{\partial x}-\frac{I_e^{\Omega^l}-I_w^{\Omega^l}}{\Delta x}\right|=\left|\frac{(1-2f_x)\Delta x}{2!}\left(\frac{\partial^2 I^{\Omega^l}}{\partial x^2}\right)\right| \tag{9}$$

In a multi-dimensional problem, the numerical scattering acts in a similar manner to the way it acted in one dimension.

Also, the fact that the spatial discretization error can be reduced only by increasing the grid numbers is not a simple problem. From Eq. (5) to Eq. (9), the radiative intensity *I* varies with the wavelength λ, based on the assumption of spectral band consistency, which affects the radiative property, i.e., $\kappa_{\alpha\lambda}$. Therefore, errors caused by the radiative property are also included in the numerical scattering within the scope. For the approximation complexity of the spectral absorption coefficient, a ratio *X* is applied to denote its deviation, which is shown in Eq. (10):

$$\kappa_{\alpha\lambda}^{*}=\chi\kappa_{\alpha\lambda} \tag{10}$$

To summarize, the factors that affect *TE* can be implemented in a correlation, which is shown in Eq. (11), which can be similarly extended to a three-dimensional problem.

$$TE = TE\left[(\Delta x, \Delta y), f_{\alpha,\beta}, \kappa^{*}_{\alpha\lambda}\right] \tag{11}$$

For brevity, the detailed explanation of the reason towards its generation can be referred in the previous works (Zhang & Tan, 2009; Tan et al., 2004; Zhang et al. 2011).

2.2 Artificial benchmark model

Consider a 2D rectangle containing an absorbing-emitting grey medium without scattering; its refractive index is uniform, and is equal to that of the surroundings. In real cases, the medium may be gaseous, solid or liquid; however, in the current work, a generalized version of the participating medium is used.

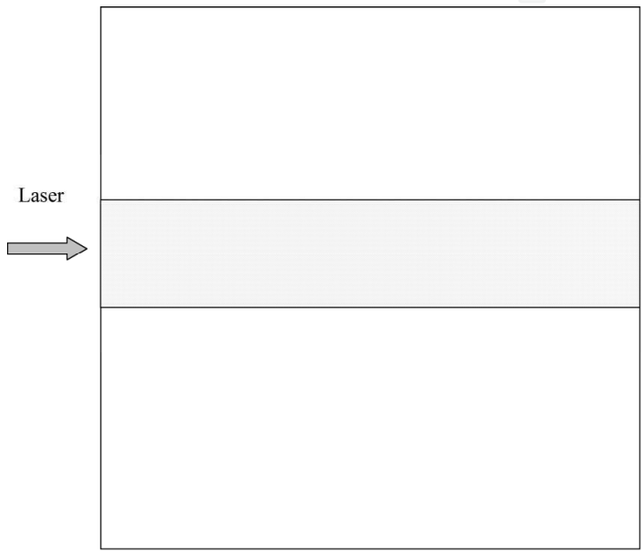

Fig. 1. Artificial benchmark model for central laser incidence to a two-dimensional rectangle

The four interfaces of the medium are all diffusely reflective, opaque and grey. Its east and west interfaces are coated with a sheet of thin film, individually. At certain wavelength, the west interface shows to be a semitransparent and specularly reflective surface. While, at other wavelengths, it is shown to be a diffusely reflective, opaque and grey surface. The thin film in its east interface is opaque, which is a diffusely reflective surface, except for the wavelength 10.6 μm. A laser beam of wavelength 10.6 μm is projected to the centre the west interface (the shadowed area), which is shown in Figure 1.

Detailed information on the current model selected can be referred in the previous works [12].

2.3 Discretization error indicator by local entropy generation rate

In case of steady state, the temperature can be determined by the following correlation, in which

$$\nabla \cdot \vec{\mathbf{q}}^{r} = \sum_{k=1}^{M_b} \kappa_k \left(4\pi I_{bk} - H_k\right) = \sum_{k=1}^{M_b} \kappa_k \left[4B_{k,T_p}\sigma T_P^4 - \sum_{\Omega^l \in 4\pi} I_k^{\Omega^l}\, \Omega^{\Omega^l}\right] \tag{12}$$

According to the expression of the local radiative entropy generation rate in a participating medium (Caldas & Semiao, 2005; Liu & Chu, 2007), an error indicator can be defined as:

$$\dot{S}'''_{gen} = \int_0^{\infty}\int_{4\pi}\left[-\left(\kappa_{a\lambda}+\kappa_{s\lambda}\right)\frac{I_\lambda(\mathbf{r},\mathbf{s})}{T_\lambda(\mathbf{r},\mathbf{s})}+\kappa_{a\lambda}\frac{I_{b,\lambda}(\mathbf{r})}{T_\lambda(\mathbf{r},\mathbf{s})}+\frac{\kappa_{s\lambda}}{4\pi}\int_{4\pi}\frac{I_\lambda(\mathbf{r},\mathbf{s}')}{T_\lambda(\mathbf{r},\mathbf{s})}\Phi(\mathbf{s}',\mathbf{s})\mathrm{d}\Omega'\right]\mathrm{d}\Omega\mathrm{d}\lambda + \int_0^{\infty}\int_{4\pi}\kappa_{a\lambda}\frac{\left[I_\lambda(\mathbf{r},\mathbf{s})-I_{b,\lambda}(\mathbf{r})\right]}{T(\mathbf{r})}\mathrm{d}\Omega\mathrm{d}\lambda \tag{13}$$

Since there is no scattering in the medium, and the refractive index is uniform, there is no refraction of the laser beam. Laser is projected from the normal direction of the west interface and when it arrives at the east interface, it is then specularly reflected to the inverse direction without angle variation. In other words, there is no scattering in the process of laser propagation through the semi-transparent in view of actual physical process; within finite time, temperature will increase only in the region where laser irradiated. When this process is simulated by numerical method and if scattering phenomenon happens, i.e., the entropy generation increasing in non-central region where the region is not irradiated by laser, numerical scattering is deemed to appear, and vise versa.

In addition, to obtain local entropy generation rate, the RTE is first solved by FVM, then it can be derived. The radiative heat transfer process in the artificial model above and the detailed derivation of the governing equation can be found in the reference (Zhang & Tan, 2009).

3. Simulation result and analysis

Radiative properties and computing parameters are: geometry of the computing domain $L_x = L_y = 0.25\,\mathrm{m}$; refractive index of medium $n = 1$, spectral absorption coefficient $\kappa_{a\lambda} = 1\,\mathrm{m}^{-1}$, spectral scattering coefficient $\kappa_{s\lambda} = 0$, and therefore, optical thickness along x and y coordinates are $\tau_x = \tau_y = 0.25$. Emissaries of the four interfaces $\varepsilon_{k,e}$, $\varepsilon_{k,w}$, $\varepsilon_{k,s}$ and $\varepsilon_{k,n}$ are uniformly specified as 0.8 and reflectivity of the four interfaces $\rho_{k,e}$, $\rho_{k,w}$, $\rho_{k,s}$ and $\rho_{k,s}$ are uniformly specified as 0.2; when $\lambda = 10.6\,\mu\mathrm{m}$, $\varepsilon_{k,w} = 0$ and $\gamma_{k,w} = 0.8$. Surrounding temperatures T_e, T_w, T_s and T_n are uniformly specified as 1000 K; initial temperature of the rectangle medium is set as T_0 = 1000 K. Moreover, the incident wavelength of the laser is set as $\lambda_{\mathrm{la}} = 10.6\,\mu\mathrm{m}$, and the power flux density of the incident laser is specified as q_{la} = 2 MW. Also, the thermal conductivity of this medium is specified to be extremely small to ensure that thermal radiation is the dominant heat transfer method.

3.1 Verification of computation code

To validate reliability and compare result of the algorithm, the following expression for temperature increment is defined as:

$$\Delta T_{i,\,j(or\,m,\,n)} = T_{i,\,j(or\,m,\,n)} - T_0 \tag{14}$$

An error indicator $EI_{\mathrm{La,T}}$ is defined as the following, which is the maximum temperature increment where node is without laser incidence region to minimum temperature increment where node is within laser incidence region, i.e.,

$$EI_{\mathrm{La,T}} = \frac{\max\left(\Delta T_{i,j}\right)\left(i, j \notin \text{Laser Incidence}\right)}{\min\left(\Delta T_{m,n}\right)\left(m, n \in \text{Laser Incidence}\right)} \tag{15}$$

Based on local entropy generation rate expression, as in shown Eq. (8), an error indicator $EI_{\mathrm{La,Sgen}}$ can be accordingly defined as:

$$EI_{\mathrm{La,\,Sgen}} = \frac{\max[\dot{S}'''_{gen}(i,j)]\,[(i,j) \subset \text{Laser Incidence}]}{\min[\dot{S}'''_{gen}\,(m,n)]\,[(m,n) \not\subset \text{Laser Incidence}]} \tag{16}$$

Both $EI_{\mathrm{La,T}}$ and $EI_{\mathrm{La,Sgen}}$ are used to evaluate numerical scattering for different situations. Since $EI_{\mathrm{La,Sgen}}$ is an absolute value for every control volume, it supplies the information of energy dissipation of the solution process, i.e., numerical dissipation, not a physically real process.

Although statistical error exists in MCM, the numerical scattering does not exist in the MCM, and its results can be used as benchmark solution to test accuracy. In MCM, the most important factor which affects its simulation accuracy is the random bundle number NM, and sensitivity of MCM with different random bundle numbers is tested, the result is shown in Tab.1, in which spatial grid number is set to $NX \times NY = 10 \times 10$.

NM	$EI_{\mathrm{La,T}}$ (%)	$EI_{\mathrm{La,Sgen}}$ (%)
10^2	2.13	0.11
10^3	1.78	0.08
10^4	0.17	0.01
10^5	0.16	0.0
10^6	0.14	0.0

Table 1. Sensitivity of MCM with different random bundle numbers

From Tab.1, it can be seen that when NM is larger than 10^4, the results of MCM is stable and less accurate, so in the following calculation, NM = 10^6 is used in all simulations. Because numerical scattering does not exist in the MCM, the results of MCM can be used as a benchmark solution to test FVM accuracy. Furthermore, the advantage of $EI_{\mathrm{La,Sgen}}$ over $EI_{\mathrm{La,T}}$ is that, as error indicators, the value of $EI_{\mathrm{La,T}}$ is affected by statistical error in MCM. Meanwhile, the value of $EI_{\mathrm{La,Sgen}}$ is independent from the statistical error in MCM. Therefore, it is shown to be a better error indicator in the current framework.

The next step is to validate the effect of solid angle discretization in FVM with several angular schemes presented, and the results are shown in Tab.2, in which spatial grid number is specified as $NX \times NY = 10 \times 10$.

In Tab.2, it can be seen that, when $N\theta \times N\varphi > 16 \times 20$, both results of $EI_{\mathrm{La,T}}$ and $EI_{\mathrm{La,Sgen}}$ is shown to be stable, and it denotes that the results of error indicator is independent from numbers of solid angle discretization grids. Therefore, in the following calculation, solid angle discretization number is set to $N\theta \times N\varphi = 24 \times 36$, which is also used in all the following simulations.

Finally, it is necessary to test the grid independence of spatial discretization number in FVM to show the uncertainty of two categories of error indicator free from spatial grid numbers. The step scheme for FVM is used, and the results are shown in Tab. 3.

$N\theta \times N\varphi$	$EI_{\mathrm{La,T}}$ (%)	$EI_{\mathrm{La,Sgen}}$ (%)
4×8	23.54	15.69
10×12	8.96	7.94
12×16	6.24	5.27
16×20	5.72	2.73
20×28	5.17	2.75
24×36	5.18	2.76

Table 2. Independence of solid angle discretization number's test

$NX \times NY$	$EI_{\mathrm{La,T}}$ (%)	$EI_{\mathrm{La,Sgen}}$ (%)
5×5	5.19	2.79
10×10	5.18	2.76
20×20	5.14	2.75

Table 3. Independence of spatial discretization numbers for FVM (step scheme)

In Tab.3, it can be seen that, when $NX \times NY > 5\times 5$, both results of $EI_{\mathrm{La,T}}$ and $EI_{\mathrm{La,Sgen}}$ is shown to be stable, which denotes that the results of error indicator is independent from numbers of spatial grids.

3.2 Numerical scattering simulation and error indicator distribution

For the case shown in Fig.1, to make the effect of numerical scattering more clear, the contours of temperature profile computed by MCM, FVM by step scheme (FVM1), FVM by diamond scheme (FVM2) and FVM by exponential scheme (FVM3) are shown in Fig.2-Fig.4.

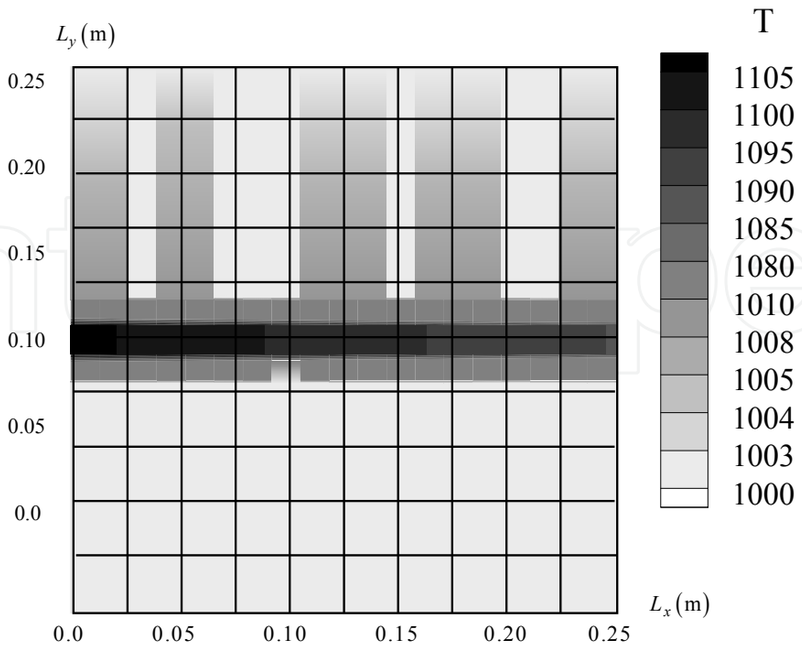

Fig. 2. Temperature contour by MCM with grid number $NX \times NY = 20\times 20$

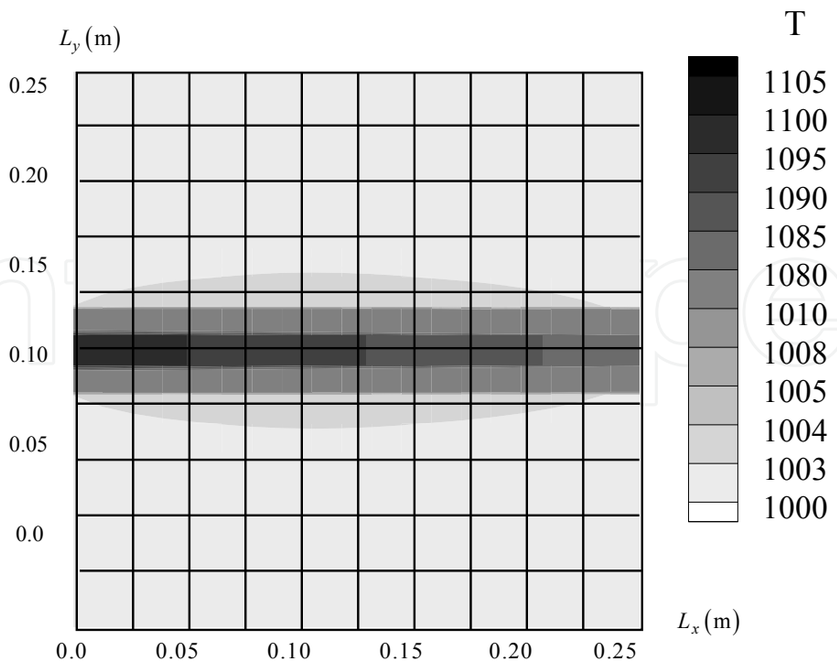

Fig. 3. Temperature contour by FVM1 with grid number $NX \times NY = 20 \times 20$

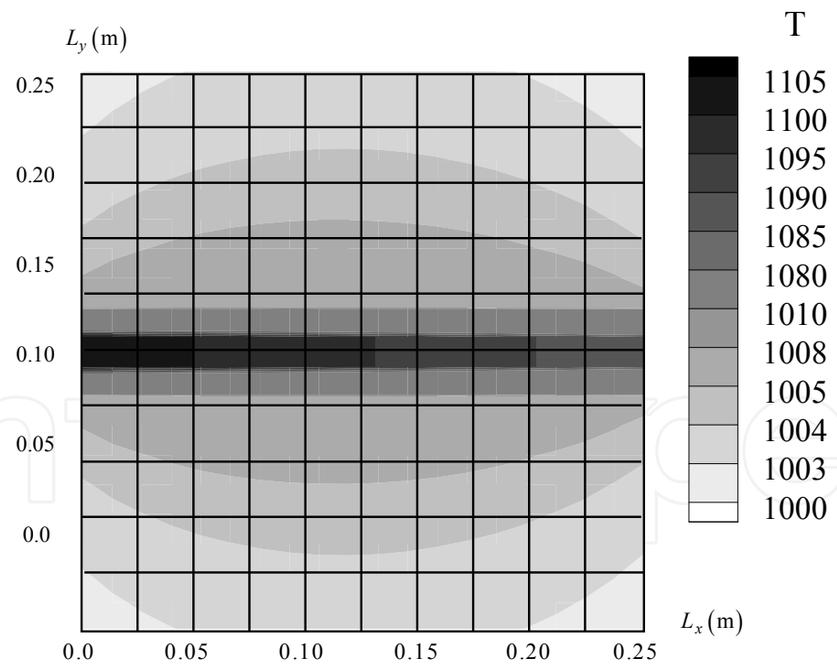

Fig. 4. Temperature contour by FVM2 with grid number $NX \times NY = 20 \times 20$

In those cases, grid number $NX \times NY = 20 \times 20$ is adopted, in which grid number of unit optical thickness is $\zeta = 80$.

The temperature distribution of each scheme in the region of laser incidence is shown in Fig.6.

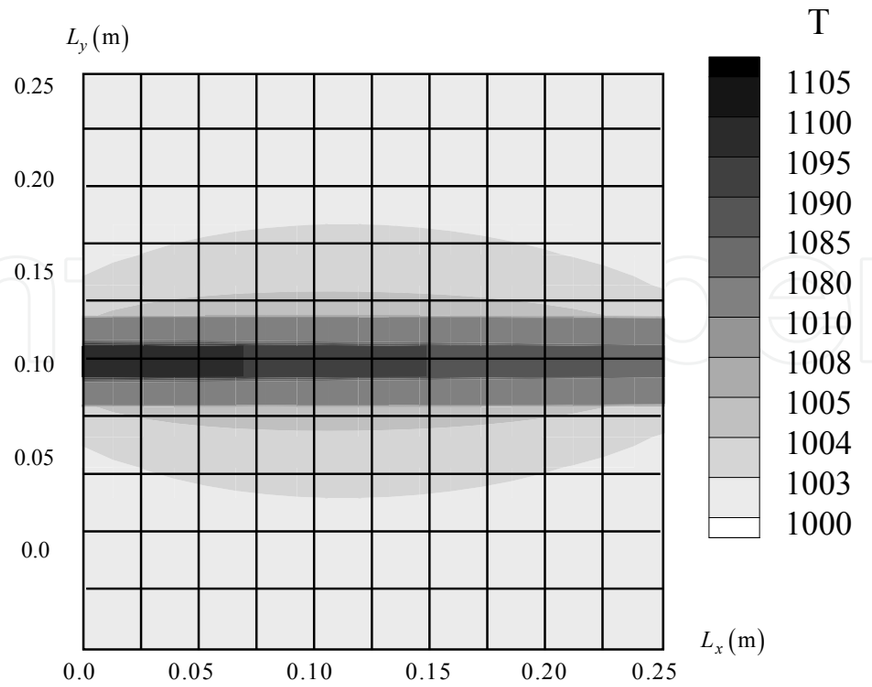

Fig. 5. Temperature contour by FVM3 with grid number $NX \times NY = 20 \times 20$

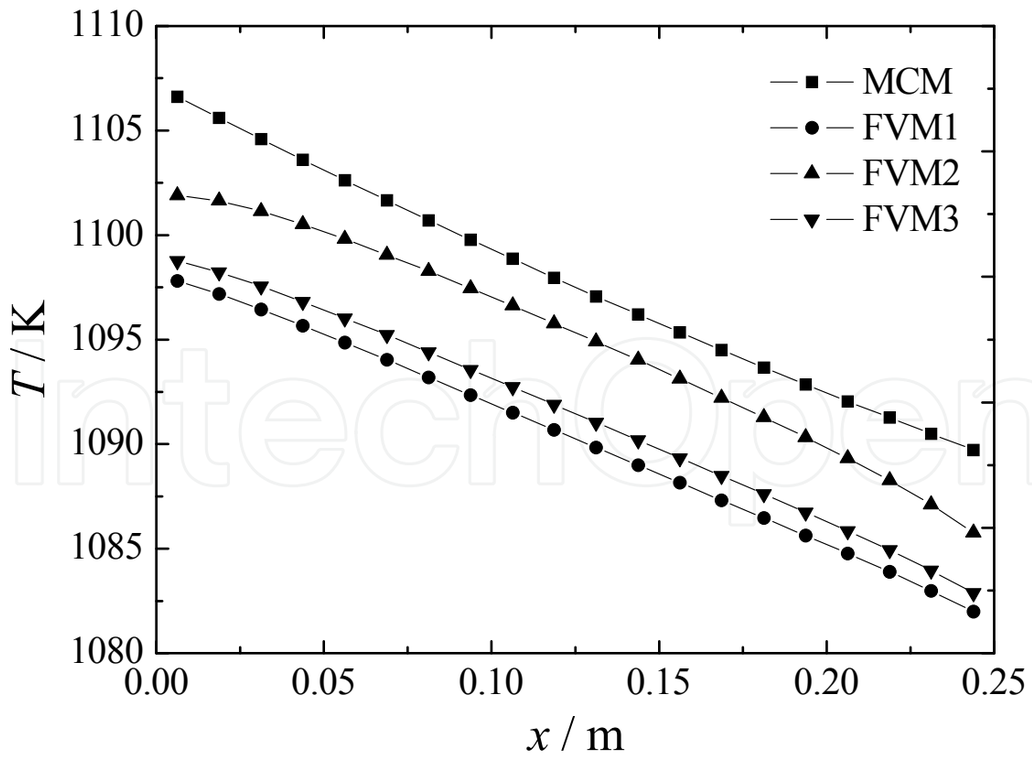

Fig. 6. Temperature profile of central laser incidence by MCM and FVM with different spatial differential schemes, $NX \times NY = 20 \times 20$

It can be seen that: among them, the accuracy of the diamond scheme is the highest, and the exponential scheme is a bit lower, the lowest accuracy of the three schemes is the step scheme.

$EI_{\mathrm{La,T}}$ for central laser incidence by MCM and FVM with different spatial differential schemes and different gird numbers is tabulated in Tab.4 .

	FVM1 (%)	FVM2 (%)	FVM3 (%)	MCM(%)
$NX \times NY = 5 \times 5 \quad Er_{\mathrm{La,T}}$	5.19	9.76	5.82	0.15
$NX \times NY = 10 \times 10 \quad Er_{\mathrm{La,T}}$	5.18	11.21	8.09	0.06
$NX \times NY = 20 \times 20 \quad Er_{\mathrm{La,T}}$	5.14	8.75	5.67	0.00

Table 4. $EI_{\mathrm{La,T}}$ for central laser incidence by MCM and FVM with different spatial differential schemes and different gird numbers

$EI_{\mathrm{La,Sgen}}$ for central laser incidence by MCM and FVM with different spatial differential schemes and different gird numbers is tabulated in Tab.5.

	FVM1 (%)	FVM2 (%)	FVM3 (%)	MCM(%)
$NX \times NY = 5 \times 5 \quad Er_{\mathrm{La,Sgen}}$	2.79	5.25	3.08	0.00
$NX \times NY = 10 \times 10 \quad Er_{\mathrm{La,Sgen}}$	2.76	5.24	3.07	0.00
$NX \times NY = 20 \times 20 \quad Er_{\mathrm{La,Sgen}}$	2.75	5.22	3.05	0.00

Table 5. $EI_{\mathrm{La,Sgen}}$ for central laser incidence by MCM and FVM with different spatial differential schemes and different gird numbers

It is also interesting to see the distribution of numerical scattering. Choosing the x-axis position where the maximum temperature increment without laser incidence happens, in different height, the distribution of numerical scattering of different spatial differential schemes with grid numbers is shown in Fig. 7.

From the Fig. 7, it is shown that, if we set the direction of laser incidence as central axis, it can be seen that numerical scattering distributed symmetry along the axis, which can be called as symmetrical cross-scattering. All of the three schemes show symmetrical cross-scattering.

It can be seen from the above tables and figures that, for grid number, when its number is increasing, numerical scattering will be reduced. This is the same tendency as in all other fields. However, on one aspect, the accuracy of FVM will also be affected by the spatial differential scheme and among them, the diamond scheme has the highest, and exponential scheme has less accuracy, while step scheme has the least accuracy of the three schemes. On the other aspect, the degree of numerical scattering is reverse, i.e., the step scheme produces minimum numerical scattering, and exponential scheme produces more, while the diamond scheme produces maximum among three methods.

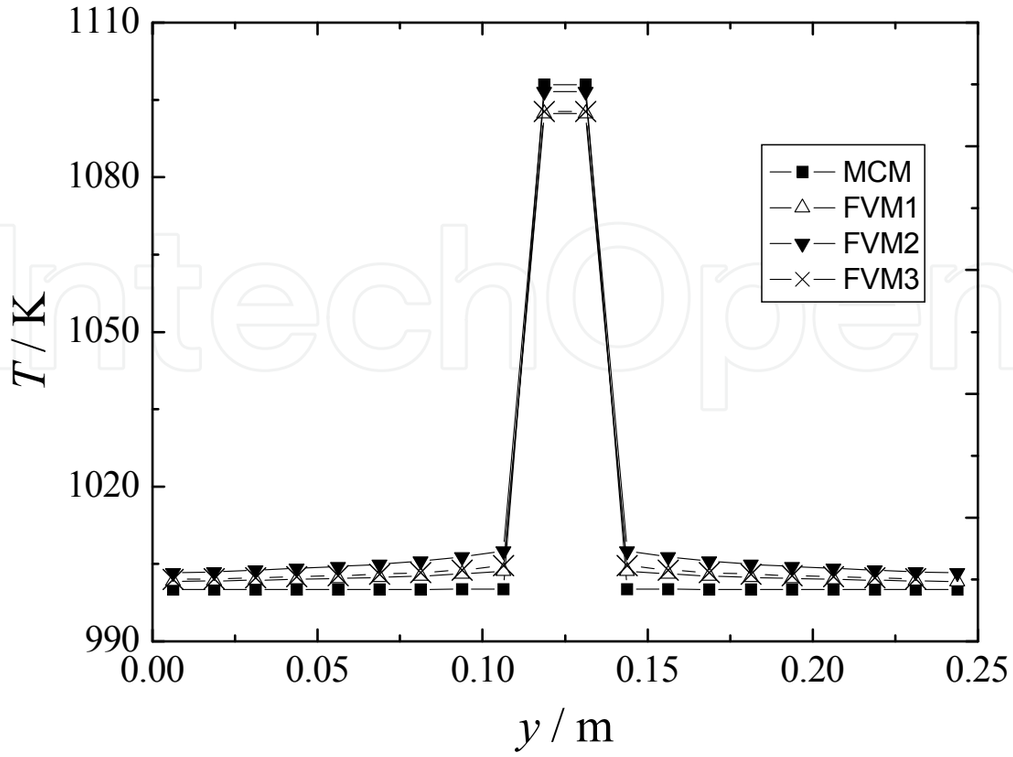

Fig. 7. Distribution of numerical scattering of FVM with different spatial differential schemes, x=0.1063, $NX \times NY = 20 \times 20$

3.3 Effect of absorption coefficients deviation

The purpose to discuss numerical scattering is to examine how to constitute better differential scheme of the intensity to obtain solution with good accuracy without less oscillation. For this reason, the hypothesis of uniform property is also included in the false scattering. By considering the individual absorption coefficients $\kappa^*_{\alpha\lambda}$ of 0.1, 1.0, 2.0 and 10.0, and the corresponding optical thicknesses τ = 0.025, 0.25, 0.5, and 2.5 individually. The numerical test results towards $EI_{\mathrm{La,T}}$ and $EI_{\mathrm{La,Sgen}}$ of grid numbers $NX \times NY = 5 \times 5$ and $NX \times NY = 20 \times 20$ for the MCMs and FVM1s are shown in Tab. 6 and Tab. 7.

$NX \times NY$	$\kappa_{\alpha\lambda}$	$Er_{\mathrm{La,T}}$ / MCM (%)	$Er_{\mathrm{La,T}}$ / FVM1 (%)
5×5	0.1	0.0	0.50
	1.0	0.15	5.17
	2.0	0.58	10.73
	10.0	23.37	65.56
10×10	0.1	0.0	0.35
	1.0	0.11	4.41
	2.0	0.49	9.51
	10.0	41.38	67.33

Table 6. $EI_{\mathrm{La,T}}$ for MCM and FVM of different absorption coefficients in central laser incidence

$NX \times NY$	$\kappa_{\alpha\lambda}$	$Er_{\mathrm{La,\,Sgen}}$ / MCM (%)	$Er_{\mathrm{La,\,Sgen}}$ / FVM1 (%)
5×5	0.1	0.0	0.02
	1.0	0.05	0.03
	2.0	0.26	9.63
	10.0	12.37	40.34
10×10	0.1	0.0	0.04
	1.0	0.03	0.12
	2.0	0.19	12.51
	10.0	9.27	59.52

Table 7. $EI_{\mathrm{La,Sgen}}$ for MCM and FVM of different absorption coefficients in central laser incidence

It can be seen that when the absorption coefficient deviation is high, the numerical scattering cannot be eliminated, even with higher grid numbers.

4. Conclusion

Based on the theory of local entropy generation rate used in fluid flow and heat transfer, an error indicator is defined to evaluate and compare discretization errors caused by different factors in FVM for solving the RTE, which is proven to be an effective approach. In addition, since the discretization error is a quality generated in the solution process, while the theory of local entropy generation is focused on process evaluation, therefore, it is shown to be better, comparing with the former error indicator defined by temperature increasing.

An artificial benchmark model of central laser incidence on a 2D rectangle containing a semi-transparent medium is proposed to investigate the numerical scattering in the FVM, along with the use of reference data from the MCM, which has been proven to generate no false scattering. Meanwhile, the value of new error indicator is independent from the statistical error in MCM.

Within the framework of the current model, it is shown that numerical scattering for the FVM is affected by the spatial grid numbers and is also affected by the different spatial discretization schemes to a large degree, with the diamond scheme being best, then the exponential scheme and finally the step scheme, in ranked order. Numerical scattering also varies with the amount of absorption coefficient deviation. When the absorption deviation is large, the numerical scattering cannot be eliminated solely by increasing the grid number. Also, numerical scattering is distributed symmetrically along the laser incidence direction, and all of the schemes show symmetrical cross-scattering.

5. Acknowledgment

The work described herein is supported by the National Natural Science Foundation of China (nos. 51006026, 90916020), the Development Program for Outstanding Young Teachers in Harbin Institute of Technology (no. HITQNJS. 2009. 022) and the Fundamental Research Funds for the Central Universities (Grant No. HIT.NSRIF. 2012072), to whom grateful acknowledgment is expressed.

6. Nomenclature

f	=	spatial differencing factor [-]
H	=	information entropy indicator [bit]
I_λ	=	spectral radiative intensity $\left[\mathrm{W}/\left(\mathrm{m}^2\text{-sr-}\mu\mathrm{m}\right)\right]$
$I_{b\lambda}$	=	blackbody spectral radiative intensity, $\left[\mathrm{W}/\left(\mathrm{m}^2\text{-sr-}\mu\mathrm{m}\right)\right]$
i, j	=	index of nodal point in the region without laser incidence [-]
NX	=	spatial discretization grid number along x axis [-]
NY	=	spatial discretization grid number along y axis [-]
$N\theta$	=	angular discretization grid number along θ direction [-]
$N\varphi$	=	angular discretization grid number along φ direction [-]
$\vec{n}_b$	=	normal vector of the boundary [-]
p	=	probability of temperature increasing due to numerical scattering [-]
$\vec{s}$	=	spatial position vector [m]
T	=	temperature [K]

Greek

γ	=	transmittance [-]
ε	=	emissivity [-]
$\kappa_{a\lambda}$	=	spectral absorption coefficient of medium [m^{-1}]
$\kappa_{s\lambda}$	=	spectral scattering coefficient of medium [m^{-1}]
λ	=	wavelength [μm]
τ	=	optical thickness [-]
Φ	=	scattering-phase function [-]
$\vec{\mathbf{\Omega}}$	=	solid angle ordinate direction [-]
$\vec{\mathbf{\Omega}}'$	=	solid angle ordinate for scattering direction [-]

Subscripts

b	=	bottom boundary of control volume p
e	=	east boundary of control volume p
i, j	=	index of nodal point in the region without laser incidence
n	=	north boundary of control volume p
p	=	control volume p
s	=	south boundary of control volume p
t	=	top boundary of control volume p
w	=	west boundary of control volume p
x, y, z	=	coordinates directions
λ	=	spectrum (wavelength)
0	=	initial value

Superscripts

Ω^l	=	a certain selected angular direction

7. References

Howell, J.R.; Siegel, R. & Menguc, M. P. (2010). *Thermal Radiation Heat Transfer* (5th Edition), CRC Press, ISBN 978-143-9805-33-6, New York, USA

Modest, M.F. (2003). *Radiative Heat Transfer* (2nd Edition), Academic Press, ISBN 978-012-5031-63-9, San Diego, USA

Shih, T. M.; Thamire, C., Sung, C. H. & Ren, A. L. (2010). Literature Survey of Numerical Heat Transfer (2000-2009): Part I. *Numerical Heat Transfer, Part A: Applications*, Vol. 57, No. 3, pp. 159-296, ISSN 1040-7782

Raithby, G. D. & Chui, E. H. (1990). A Finite-Volume Method for Predicting a Radiant Heat Transfer in Enclosures with Participating Media, *ASME Transactions Journal of Heat Transfer*, Vol. 112, pp. 415-423, ISSN 0022-1481

Borjini, M. N.; Guedri, K. & Said R. (2007). Modeling of Radiative Heat Transfer in 3D Complex Boiler with Non-gray Sooting Media, *Journal of Quantitative Spectroscopy & Radiative Transfer*, Vol. 105, No. 2, pp. 167-179, ISSN 0022-4073

Das, R.; Mishra, S. C.; Ajith M.; et al. (2008). An inverse analysis of a transient 2-D conduction-radiation problem using the Lattice Boltzmann method and the finite volume method coupled with the genetic algorithm, *Journal of Quantitative Spectroscopy & Radiative Transfer*,Vol.109, No.11, pp. 2060-2077, ISSN 0022-4073

Farzad, B.T. & Shahini, M. (2009). Combined Mixed Convection-Radiation Heat Transfer within a Vertical Channel: Investigation of Flow Reversal, *Numerical Heat Transfer Part A: Applications*, Vol. 55, No. 3, pp. 289-307, ISSN 1040-7782

Han, S. H.; Baek, S. W. & Kim, M. Y. (2009). Transient Radiative Heating Characteristics of Slabs in a Walking Beam Type Reheating Furnace, *International Journal of Heat and Mass Transfer*, Vol. 52, No. 3, pp. 1005-1011, ISSN 0017-9310

Kim,C.; Kim, M.Y.; Yu M.J. & Mishra S.C. (2010). Unstructured Polygonal Finite-Volume Solutions of Radiative Heat Transfer in a Complex Axisymmetric Enclosure, *Numerical Heat Transfer Part B: Fundamentals*, Vol. 57, No. 3, 2010, pp. 227-239, ISSN 1040-7790

Daniel, R. R. & Fatmir, A. (2011). A consistent interpolation function for the solution of radiative transfer on triangular meshes. I-comprehensive formulation, Numerical *Numerical Heat Transfer Part B: Fundamentals*, Vol. 59, No. 2, pp. 97-115, ISSN 1040-7790

Chai, J. C.; Lee, H. S. & Patankar, S. V. (1993). Ray effect and false scattering in the discrete ordinates method, *Numerical Heat Transfer Part B: Fundamentals*, Vol. 24, No. 4, pp. 373-389, ISSN 1040-7790

Zhang, H. C. & Tan, H. P. (2009). Evaluation of Numerical Scattering in Finite Volume Method for Solving Radiative Transfer Equation by a Central Laser Incidence Model, *Journal of Quantitative Spectroscopy & Radiative Transfer*, Vol. 110, No. 18, pp. 1965-1977, ISSN 0022-4073

Patankar, S. V. (1980). *Numerical Heat Transfer and Fluid Flow*, Hemisphere Pub, ISBN 978-089-1165-22-4, Washington, DC, USA

Tan, H. P.; Zhang, H.C. & Zhen, B. (2004). Estimation of Ray Effect and False Scattering in Approximate Solution Method for Thermal Radiative Transfer Equation, *Numerical Heat Transfer Part A: Applications*, Vol. 46, No. 8, pp. 807-829, ISSN 1040-7782

Kallinderis, Y. & Kontzialis, C. (2009). A Priori Mesh Quality Estimation via Direct Relation between Truncation Error and Mesh Distortion, *Journal of Computational Physics*, Vol. 228, No. 3, pp. 881-902, ISSN 0021-9991

Coelho, P. J. (2008). A Comparison of Spatial Discretization Schemes for Differential Solution Methods of the Radiative Transfer Equation, *Journal of Quantitative Spectroscopy & Radiative Transfer*, Vol. 109, No. 2, pp. 189-200, ISSN 0022-4073

Kamel, G.; Naceur, B. M.; Rachid M. & Rachid S. (2006). Formulation and Testing of the FTn Finite Volume Method for Radiation in 3-D Complex Inhomogeneous Participating Media, *Journal of Quantitative Spectroscopy & Radiative Transfer*, Vol. 98, No. 3, pp. 425-445, ISSN 0022-4073

Naterer, G. F. & Camberos J. A. (2003). Entropy and the Second Law Fluid Flow and Heat Transfer Simulation, *AIAA Journal of Thermophysics and Heat Transfer*, Vol. 17, No. 3, 2003, pp. 360-371, ISSN 0887-8722

Camberos, J. A. (2000). The Production of Entropy in Relation to Numerical Error in Compressible Viscous Flow, *AIAA Paper*, No. 2000-2333, AIAA Fluid 2000 Symposium, Denver, CO, June, 2000

Cover, T. M. & Thomas, J. A. (2003). *Elements of Information Theory*, Tshinghua University Press, ISBN 730207285X, Beijing, China

Camberos, J. A. (2007). A Review of Numerical Methods in Light of the Second Law of Thermodynamics, 39th AIAA Thermophysics Conference, 25-28, June 2007, Miami, FL: 410-444.

Caldas, F. & Semiao, V. (2005). Entropy Generation through Radiative Transfer in Participating Media: Analysis and Numerical Computation, *Journal of Quantitative Spectroscopy & Radiative Transfer*, Vol. 96, No.3-4, pp. 423-437, ISSN 0022-4073

Liu L. H. & Chu S. X. (2007). Verification of Numerical Simulation Method for Entropy Generation of Radiation Heat Transfer in Semitransparent Medium, *Journal of Quantitative Spectroscopy & Radiative Transfer*, Vol. 103, No. 1, pp. 43-56, ISSN 0022-4073

Zhang, H. C.; Tan H. P. & Li Y. (2011). Numerical Uncertainty for Radiative Transfer Equation by an Information Entropy Approach, *AIAA Journal of Thermophysics and Heat Transfer*, Vol. 25, No. 4, pp. 635-638, ISSN 0887-8722

Herwig, H. & Kock, F. (2004). Local entropy production in turbulent shear flows: A high-Reynolds number model with wall functions, *International Journal of Heat and Mass Transfer*, Vol. 47, No. 10-11, pp. 2205-2215, ISSN 0017-9310

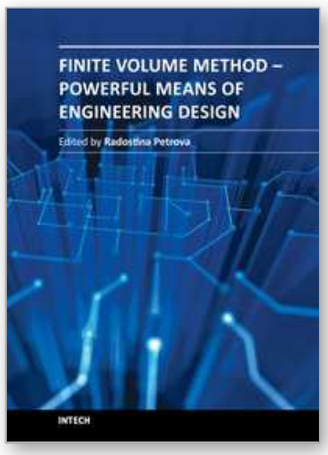

Finite Volume Method - Powerful Means of Engineering Design
Edited by PhD. Radostina Petrova

ISBN 978-953-51-0445-2
Hard cover, 370 pages
Publisher InTech
Published online 28, March, 2012
Published in print edition March, 2012

We hope that among these chapters you will find a topic which will raise your interest and engage you to further investigate a problem and build on the presented work. This book could serve either as a textbook or as a practical guide. It includes a wide variety of concepts in FVM, result of the efforts of scientists from all over the world. However, just to help you, all book chapters are systemized in three general groups: New techniques and algorithms in FVM; Solution of particular problems through FVM and Application of FVM in medicine and engineering. This book is for everyone who wants to grow, to improve and to investigate.

How to reference
In order to correctly reference this scholarly work, feel free to copy and paste the following:

H. C. Zhang, Y. Y. Guo, H. P. Tan and Y. Li (2012). A Concept of Discretization Error Indicator for Simulating Thermal Radiation by Finite Volume Method Based on an Entropy Generation Approach, Finite Volume Method - Powerful Means of Engineering Design, PhD. Radostina Petrova (Ed.), ISBN: 978-953-51-0445-2, InTech, Available from: http://www.intechopen.com/books/finite-volume-method-powerful-means-of-engineering-design/a-concept-of-discretization-error-indicator-for-simulating-thermal-radiation-by-finite-volume-method

INTECH
open science | open minds

InTech Europe
University Campus STeP Ri
Slavka Krautzeka 83/A
51000 Rijeka, Croatia
Phone: +385 (51) 770 447
Fax: +385 (51) 686 166
www.intechopen.com

InTech China
Unit 405, Office Block, Hotel Equatorial Shanghai
No.65, Yan An Road (West), Shanghai, 200040, China
中国上海市延安西路65号上海国际贵都大饭店办公楼405单元
Phone: +86-21-62489820
Fax: +86-21-62489821

IntechOpen